Optica Applicata, Vol. XXXIV, No. 4, 2004

Multimode interference structures – properties and applications

MAREK BŁAHUT[1], DAMIAN KASPRZAK[2]

[1]Institute of Physics, Silesian University of Technology, ul. Bolesława Krzywoustego 2, 44-100 Gliwice, Poland; e-mail: blahut@zeus.polsl.gliwice.pl

[2]PWPT WASKO, ul. Berbeckiego 6, 44-100 Gliwice, Poland; e-mail: d.kasprzak@wasko.pl

The aim of this paper is to present operating principles and properties of multimode interference (MMI) structures and their basic applications in optoelectronic circuits. We discuss the principles of direct, mirrored and multiple image formation for the general and restricted interference. We also show the possibility of self-imaging effects in gradient index waveguides. Based on the above, we present MMI applications in splitters and couplers $N\times M$ technology of different configurations, Mach–Zehnder interferometers (MZI) and phase shifters.

Keywords: MMI structures, ion-exchange, integrated optics.

1. Introduction

When we excite a multimode waveguide, we can observe the effects involving the matching of input field with mode fields of the multimode waveguide, and then the interference of the waves produced. The intermode interference is accompanied by so-called self-imaging effects of input field which is exciting the multimode waveguide. As a result of these effects, the input field, which most frequently comes from a single mode waveguide, or from a group of single mode waveguides, is reproduced as direct, mirrored and multiple images. This phenomenon constitutes a basis for the operation of multimode interference (MMI) structures.

The development of the systems of integrated optics making use of MMI and based on step-index optical waveguides, and in particular, systems based on semiconductor structures, can be observed since the early 1990s [1], [2]. In works [3], [4] it has been affirmed that the self-imaging effects can occur in gradient waveguides produced by ion exchange method.

2. Operating principles

The scheme of MMI structure is shown in Fig. 1. It consists of a group of monomode waveguides (*a*), which define the input field, a wide multimode section (*b*) (typically monomode in *Y* direction), where the interference effects of modal fields are observed, and output monomode waveguides (*c*).

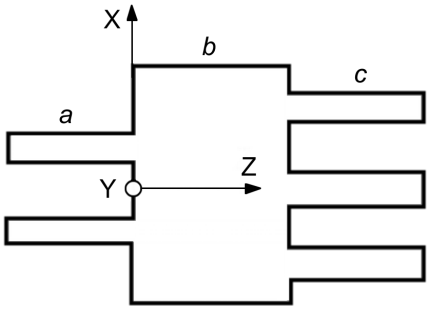

Fig. 1. Scheme of MMI structure.

The monomode waveguides give stable distribution of the input field E for $z = 0$. This field introduced to interference section is decomposed into the modal functions φ_{l0} of all modes of multimode waveguide:

$$E(x, y, 0) = \sum_l c_{l0}\varphi_{l0}(x, y), \qquad c_{l0} = \frac{\int E(x, y, 0)\,\varphi_{l0}(x, y)\,\mathrm{d}x\,\mathrm{d}y}{\sqrt{\int \varphi_l^2(x, y)\,\mathrm{d}x\,\mathrm{d}y}} \tag{1}$$

where φ_{l0} is the orthogonal wave function of (l, 0) mode with propagation constant β_{l0} and c_{l0} are the excitation coefficients.

Each mode of MMI section propagates with a different phase velocity and hence the field at the distance z is a superposition of all modal fields with the same excitation coefficients and different phase shifts (we omit unimportant index 0):

$$E(x, y, z) = \sum_l c_l\varphi_l(x, y)\exp(-j\beta_l z). \tag{2}$$

As a result, we observe the interference pattern which changes with the propagation length.

The interference pattern observed in the MMI section depends on mode properties of multimode waveguide. Of particular importance is the dependence of propagation constants β_l on the mode number. For step-index waveguides it is nearly quadratic and so-called self-imaging effects are observed and the input field is reproduced in direct, mirrored and multiple images.

A similar quadratic dependence of the propagation constants on mode number is also observed in waveguides obtained by silver-sodium and potassium-sodium ion-exchange [3]:

$$\beta_l = A + Bl(l+2), \tag{3}$$

where A, B = const, so we can expect the self-imaging effects to appear in gradient -index waveguides obtained in this technology.

According to the theory presented in paper [2] for step-index waveguides the beat length L_z of the two lowest order modes have to be defined

$$L_z = \frac{\pi}{\beta_0 - \beta_1} \quad \Rightarrow \quad \beta_0 - \beta_1 = \frac{l(l+2)\pi}{3L_z}. \tag{4}$$

Substituting this dependence to Eq. (2), describing the field at the distance z in which the phase of fundamental mode is taken out of the sum as a common factor

$$E(x, y, z) = \exp(-j\beta_0 z)\sum_l c_l \varphi_l(x, y)\exp\left(j\frac{l(l+2)\pi}{3L_z}z\right) \tag{5}$$

it can be easily shown that in the case where the propagation length z obeys relation:

$$z = n(3L_z) \quad \Rightarrow \quad \exp\left(j\frac{l(l+2)\pi}{3L_z}z\right) = \begin{cases} 1 & n-\text{even} \\ (-1)^l & n-\text{odd} \end{cases} \tag{6}$$

the field distributions, with accuracy to the constant phase factor, are described by the equations:

$$\begin{aligned} E\left(x, y, n(3L_z)\right) &= E(x, y, 0) \quad \Leftrightarrow \quad n-\text{even}, \\ E\left(x, y, n(3L_z)\right) &= E(-x, y, 0) \quad \Leftrightarrow \quad n-\text{odd}. \end{aligned} \tag{7}$$

The first distribution is a *direct* replica of the input field and the second is an image *mirrored* with respect to the waveguide axis of symmetry. The dependences depicted describe the so-called general interference.

It can also be shown that for the input positions – symmetrical and at 1/3 and 2/3 of the waveguide width, waveguide modes are selectively excited. It is the case of the so-called restricted interference.

In Fig. 2, calculated modal field distributions of MMI section made by the potassium-sodium ion-exchange are presented. The diffusion window position and the excitation position – symmetrical and at 1/3 of the window are marked. It can be noticed

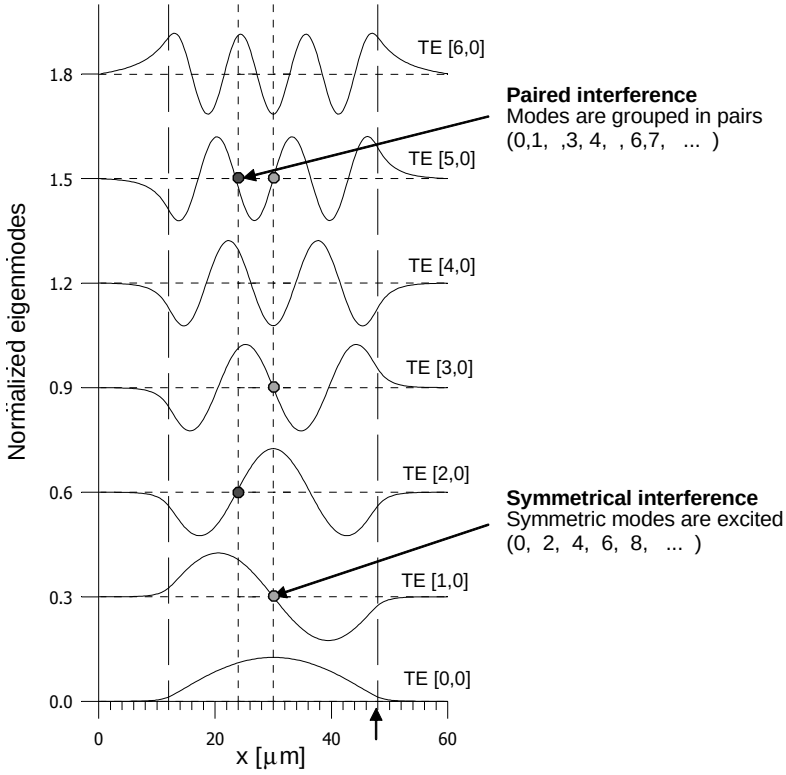

Fig. 2. Normalized modal fields of MMI section made by K^+-Na^+ ion exchange (window width 36 μm, TE modes).

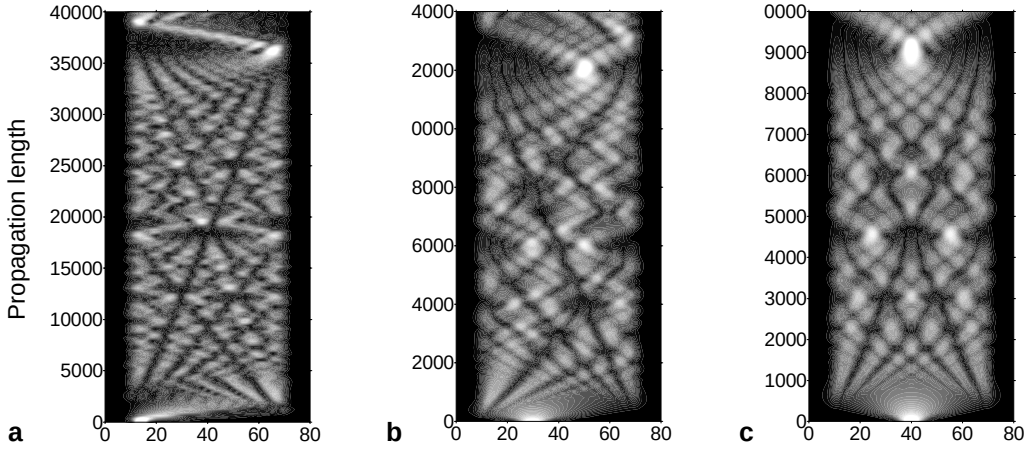

Fig. 3. Field evolution of TE wave in MMI section made by K^+-Na^+ ion exchange for the window width 60 μm and time of diffusion 1 h (dimensions in μm): **a** – for arbitrary asymmetric excitation (general interference), **b** – for asymmetric excitation at 1/3 of the waveguide width (paired interference), **c** – for symmetric excitation (symmetric interference).

that in the first case only symmetrical modes are excited and for any symmetrical mode number l the condition $l(l + 2) = 4N$ ($N = 1, 2, \ldots$) is satisfied. This allows observing the self-imaging effects for the propagation length of the four times shorter, simple and reflected images appear now at $z = n(3/4 \cdot L_z)$. It is so-called symmetric interference [1]. In the second case, the input field does not excite modes numbered 2, 5, 8, … and the others are grouped in pairs. This shortens the propagation length required for self-imaging three times (simple and reflected images appear for $z = nL_z$). The interference described is called a paired interference [1].

Figure 3 presents examples of interference pattern for arbitrary asymmetric excitation (general interference) – Fig. 3**a**, for asymmetric excitation at 1/3 of the waveguide width (paired interference) – Fig. 3**b**, for symmetric excitation (symmetric interference) – Fig. 3**c**. Beam propagation method (BPM) calculations were performed for gradient index MMI section made by potassium-sodium ion-exchange [4]. Propagation lengths for direct and mirrored images obey expected relations:

$$L \text{ (general)} = 3L \text{ (paired)} = 4L \text{ (symmetric)}. \tag{8}$$

3. Experimental investigation of MMI structures

Experimental investigation of MMI structures is performed in experimental stand shown in Fig. 4 [5]. The MMI section, excited from laser is covered with fluorescent substance (Nile Blue "A") by spin-coating. The evanescent waves of mode fields, penetrating the layer of fluorescent substance, force fluorescence proportionally to the energy of excited mode. This distribution is recorded by a sensitive CCD camera and then registered and analyzed in a computer. We used this stand to examine gradient index MMI structures made by ion exchange process. Recording successive sequences of mode field interference patterns makes it possible to determine the dependence of propagation lengths for N-fold images on different technological parameters. For ion exchange these are window width, time and temperature of diffusion.

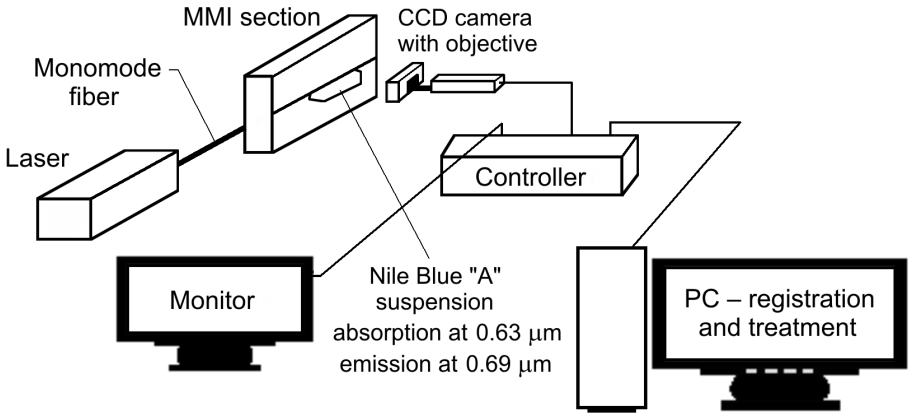

Fig. 4. Scheme of the experimental stand.

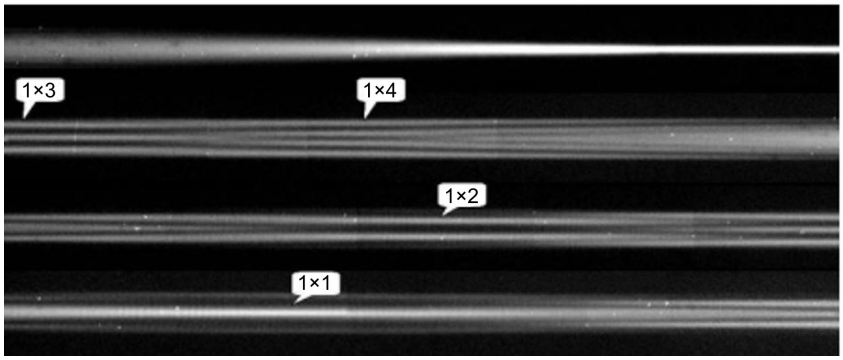

Fig. 5. Successive sequences of recorded mode field interference images for MMI section of the width 36 μm, made by K^+-Na^+ ion exchange, symmetrically excited.

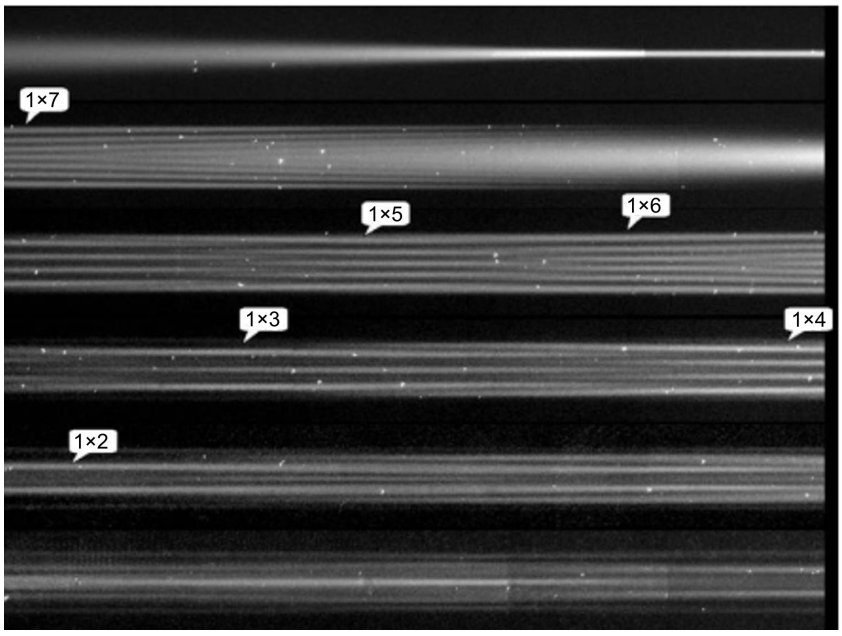

Fig. 6. Successive sequences of recorded mode field interference images for MMI section of the width 60 μm, made by K^+-Na^+ ion exchange, symmetrically excited.

The proposed method for investigation of MMI structures enables a complete analysis of their properties. Figure 5 presents (see [5], for instance) successive sequences of recorded mode field interference images for gradient index MMI section made by potassium-sodium ion exchange for the window width 39 μm, which guides 7 modes. The input field coming out from the single-mode waveguide extends as a result of diffraction, achieving waveguide boundaries. Then, during successive reflections, the field matches the mode structure and next the evolution of interference

patterns along the propagation length is observed. For the section under study, distinctly visible are 1×4, 1×3, 1×2 and 1×1 self-images marked in the interference pattern. In a wider section of the width 60 μm, which guides 11 modes, it is also possible to observe 1×6, 1×5, 1×4 *N*-fold images (Fig. 6).

The TE and TM waveguide modes which appear in MMI section for the excitation by the unpolarized field from single-mode fibre have different modal characteristics depending on propagation conditions at the substrate surface. Additionally, the material birefringence is observed for waveguides obtained by potassium-sodium ion exchange,

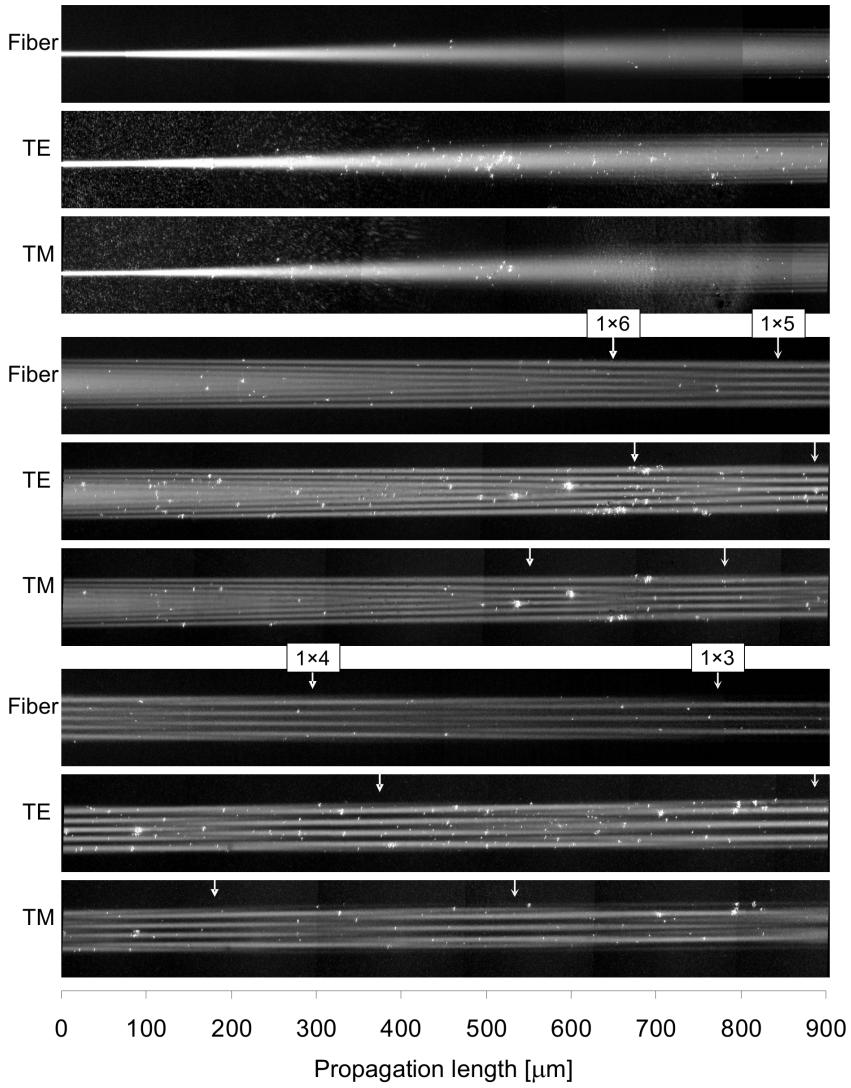

Fig. 7. Successive sequences of recorded mode field interference images for MMI section of the width 60 μm, made by K^+-Na^+ ion exchange, symmetrically excited by TE, TM waves and unpolarized light.

caused by stresses produced in the technological process – maxima of the refractive index change are different for TE and TM modes. For these reasons, the differences in interference patterns for both polarizations should exist [6]. As can be seen in Fig. 7, *N*-fold images appear at different propagation lengths, *i.e.*, shorter for TM , longer for TE and in intermediate position for unpolarized light.

4. Applications

Unique properties of MMI structures such as insensitivity to wavelength, low loss, small size and ease of fabrication make them attractive for applications in couplers or splitters technology of different configurations [7], [8], [9], [10], Mach–Zehnder interferometers (MZI) and passive phase shifters, modulators and switches [11] and wavelength division multiplexers [12], [13].

Using the self-imaging effects of input field power 1×*N* and *N*×*M* splitters and couplers can be produced, having very good optical parameters, where the branching of input field is realized over a very small area of a few hundred μm. MMI splitters and couplers were developed in step index configuration including gallium arsenide, aluminum silicate on silicon, indium phosphate, and silica on silicon [7], [8].

MMI couplers/splitters can also be produced in gradient index waveguides technology. In the work [14] the technology of waveguide splitters made by silver-sodium ion-exchange was presented. In this paper, we present waveguide splitters made by potassium-sodium ion exchange. Splitters were produced during 1 h and at a

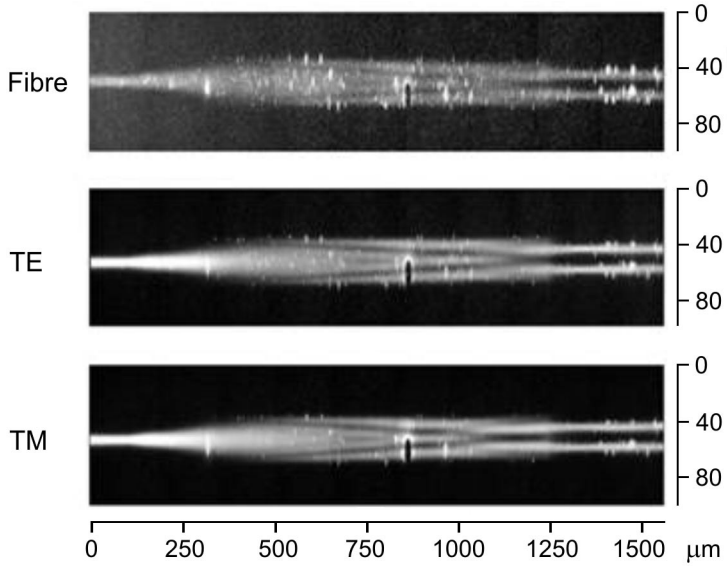

Fig. 8. Successive sequences of recorded mode field interference images for 1×2 MMI splitter of the width 30 μm.

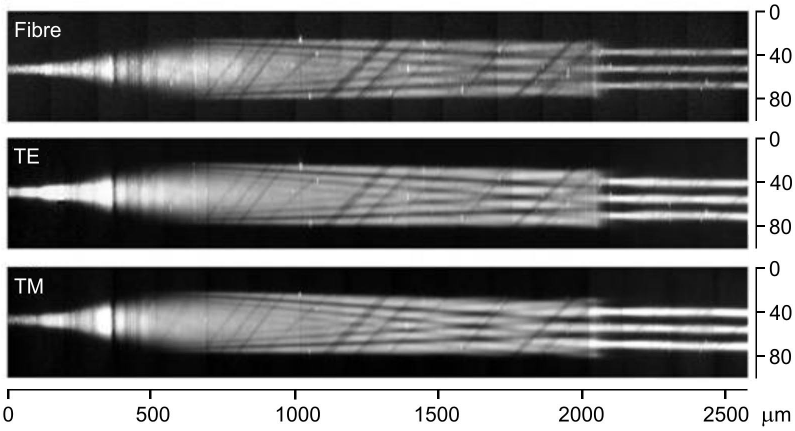

Fig. 9. Successive sequences of recorded mode field interference images for 1×3 MMI splitter of the width 51 μm.

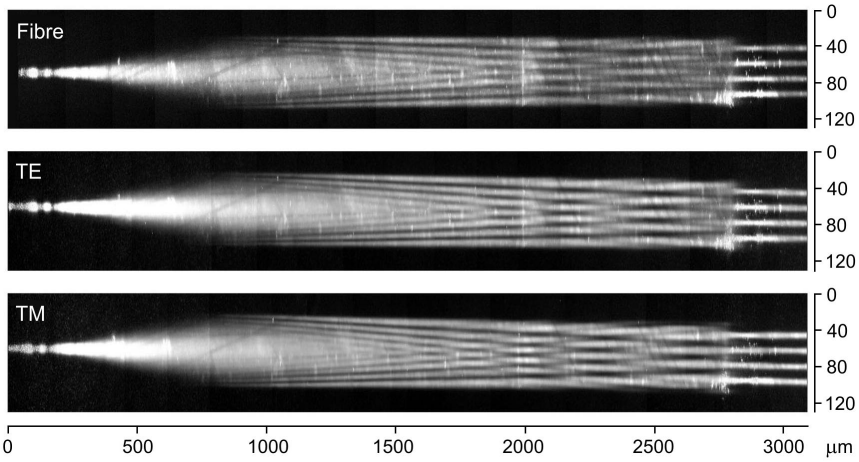

Fig. 10. Successive sequences of recorded mode field interference images for 1×4 MMI splitter of the width 69 μm.

temperature of 400 °C in BK-7 glass. The images (Figs. 8–10) visualize how 1×2, 1×3 and 1×4 splitters operate in symmetrical configuration. Transverse dimensions are enlarged four times in relation to longitudinal dimensions. Splitters are excited by TE wave, TM wave and unpolarized light. Measurements of the field distribution at their outputs presented in Tab. 1, show that the field introduced is uniformly distributed at their outputs.

MMI optical waveguide couplers and splitters can be used in MZI technology of different configurations. A diagram of the simplest MZI structure is presented in Fig. 11**a**. It consists of a pair of symmetrical MMI structures working as a 1×2

T a b l e 1. Output/input signals ratio of 1×*N* splitters.

	Splitter 1×2		Splitter 1×3			Splitter 1×4			
Output arms	I_1	I_2	I_1	I_2	I_3	I_1	I_2	I_3	I_4
Output/input signals ratio I_i/I_0	0.49	0.51	0.33	0.33	0.34	0.27	0.24	0.23	0.26

waveguide splitter and coupler, respectively, connected through the interferometer arms of the length L_A and separation distance W_A. Figure 11**b** showns the field evolution in gradient index interferometer made by silver-sodium ion-exchange for geometrical parameters listed below. Excess loss of the device is equal to about 1 dB.

Using Mach–Zehnder configuration it is possible to make MMI splitters in configuration that allows free selection of the power splitting ratios at the output.

In the works [9], [10] there have been presented 1×2 waveguide beam splitters of an arbitrary distribution of a signal at the output, made using the technology based on silicon. In the configuration considered in [9] use is made of the curved MMI section,

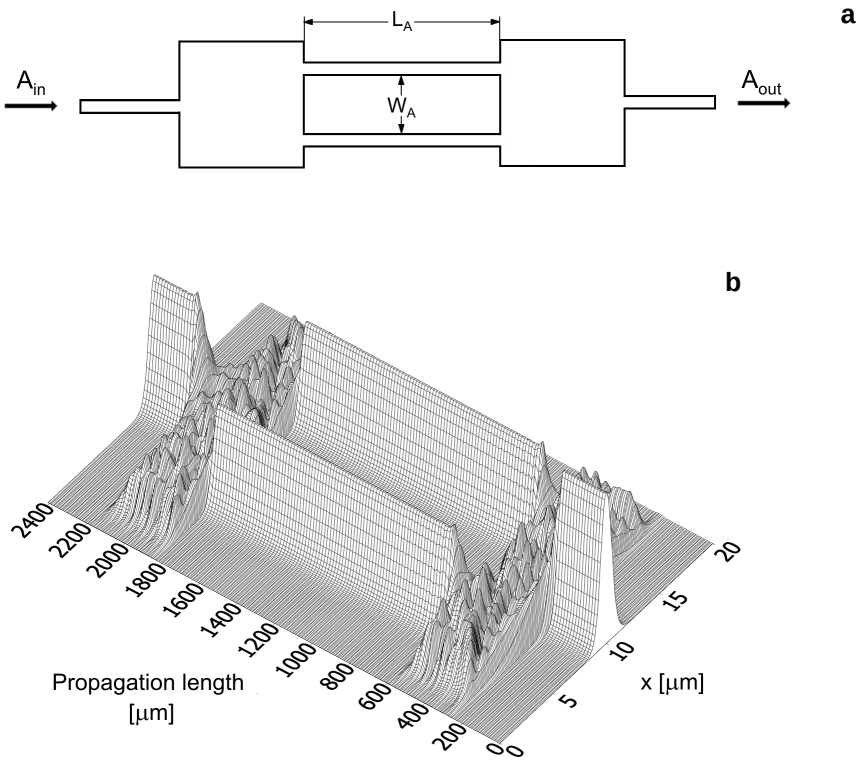

Fig. 11. Mach–Zehnder interferometer based on MMI structures made by Ag^+-Na^+ ion exchange: the scheme of configuration (**a**), TE wave propagation (**b**).

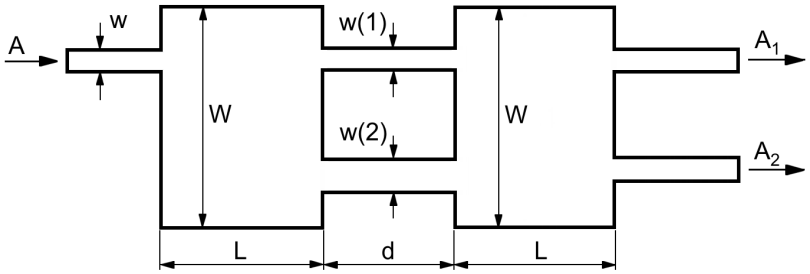

Fig. 12. Scheme of a splitter operating with an arbitrary power division at the output.

which allows obtaining an arbitrary distribution of the signal at the output. Turning the 1×2 beam splitter through a certain angle with respect to the original direction of propagation may cause problems while designing other elements of the optoelectronic circuit. The 1×2 beam splitter system presented in [10] makes use of two MMI sections working as 3 dB couplers. In the area between the MMI sections, apart from the waveguide joining them, there is a gap filled with base material. Due to the difference in the refractive indexes of the waveguide core and the base, the waves reaching the second MMI section are out of phase. And consequently, the ratio of signals at the output is the function of the gap's length. However, the above solution has a weak point that is the excess loss of the structure connected with the diffraction of the field within the gap area, which is rising along with its length.

In Figure 12, a 1×2 waveguide beam splitter has been proposed, based on gradient MMI structures with an arbitrary power splitting ratio at the output. The beam splitter consists of two asymmetrical gradient MMI sections working as 3 dB couplers or splitters, joined together with monomode waveguides of the different window width of the length L, made by silver-sodium ion exchange in glass (MZI configuration).

The differences in the widths of waveguides result in different values of propagation constants β_1^0, β_2^0 and connected with this phase changes $\Delta\phi$ at the input of the second MMI section. The optical powers I_1 and I_2 in the output arms can be expressed by the equations [15]:

$$I_1 \sim A_1^2 = A^2 \sin^2 \Delta\phi, \qquad I_2 \sim A_2^2 = A^2 \cos^2 \Delta\phi, \qquad \Delta\phi = L(\beta_1^0 - \beta_2^0) \tag{9}$$

where A, A_1, A_2 denote amplitude modulus at the input and output, respectively. The operating characteristics of the 1×2 beam splitters have been determined for different geometry configurations of waveguides joining the MMI sections [15]. Figure 13 presents sample characteristic of the device.

The self-imaging effects in MMI structures make it possible to use in one of the interferometer arms a multimode waveguide if only its length is equal to the coupling length for single self-imaging.

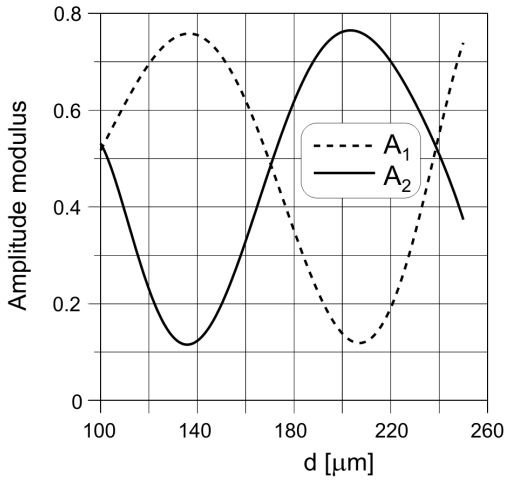

Fig. 13. Absolute values of output amplitudes A_1 and A_2 as functions of the waveguide length d for w = 0.9 μm, $w(1)$ = 0.9 μm, $w(2)$ = 1.2 μm.

In order to analyse the functioning of a multimode element in the coupling region we introduce from Eq. (5) the field distribution $E(x, y, z)$ at the distance z:

$$E(x, y, z) = \exp(-j\beta_{M0}z)\sum_l c_l\varphi_l(x, y)\exp\left(j\frac{l(l+2)\pi}{3L_z}z\right) \tag{10}$$

where β_{M0} is the propagation constant of the fundamental mode of multimode waveguide. Hence, for the distance z corresponding to the coupling length for one-fold images (Eq. 6):

$$E(x, y, z) = \exp(-j\beta_{M0}z)\sum_l c_l\varphi_l(x, y) = \exp(-j\beta_{M0}z)E(x, y, 0) \tag{11}$$

where $E(x, y, 0)$ is the field distribution at the beginning of multimode waveguide (Fig. 14). The phase shift that determines the optical powers I_1 and I_2 in output arms

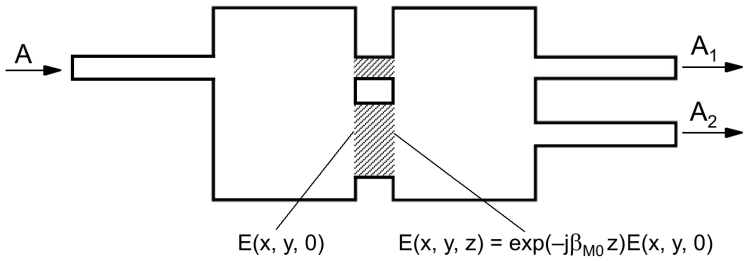

Fig. 14. Scheme of an interferometer with a multimode waveguide in the coupling region.

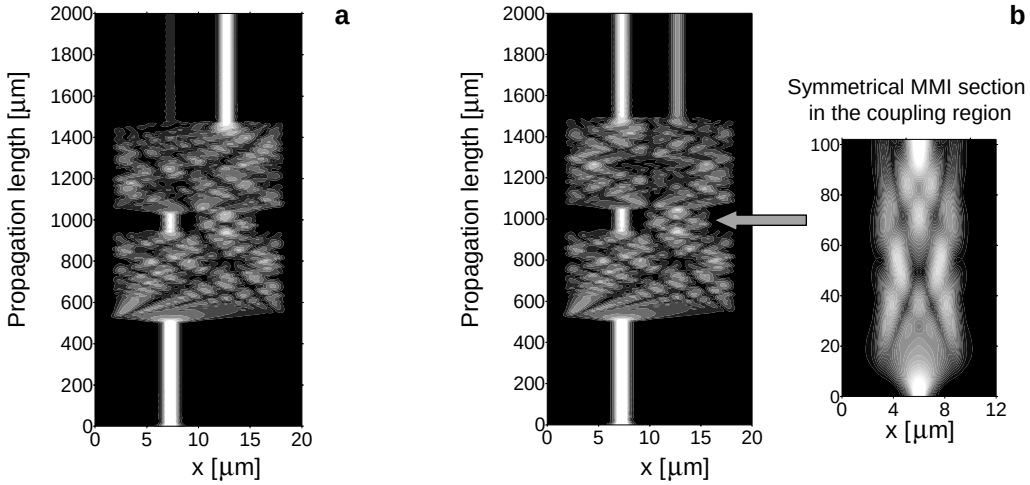

Fig. 15. Contour maps of the field amplitude distribution along the propagation length in the beam splitter structure with multimode waveguide in the coupling region for the window width: **a** – 5.5 μm (L = 87 μm), and **b** – 6 μm (L = 102 μm).

depends now on the difference of propagation constant of single-mode waveguide β_0 and propagation constant of fundamental mode of multimode waveguide β_{M0}:

$$\Delta\phi = (\beta_{M0} - \beta_0)L \tag{12}$$

where L is the length of the self-image formation. Figure 15 shows a sample field evolution of TE wave in MMI splitter under examination for the input and output

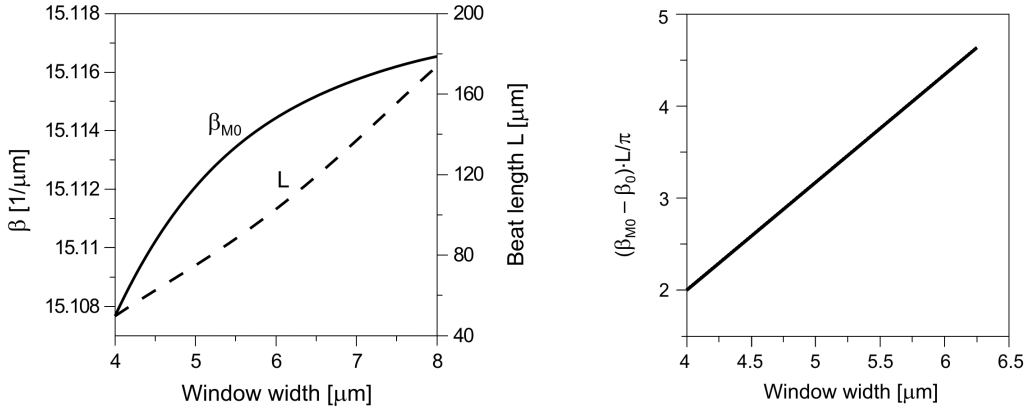

▲

Fig. 16. Dependence of propagation constant of the fundamental mode of multimode waveguide β_{M0} and the coupling length for the self-image formation on the multimode waveguide width.

Fig. 17. Phase difference as a function of the waveguide width.

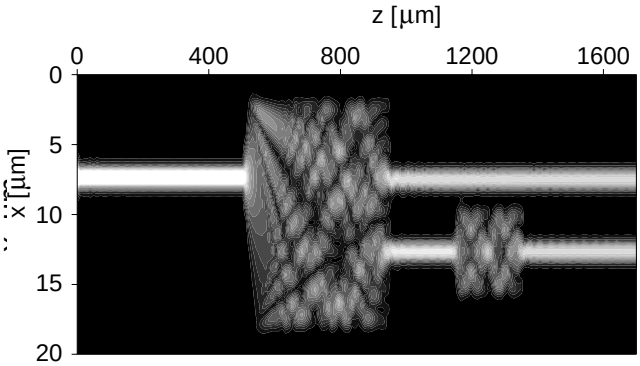

Fig. 18. Field evolution in the phase shifter made by silver-sodium ion-exchange.

T a b l e 2. Geometrical parameters of the π radians phase shifter optimized to work at a wavelength of 0.63 μm.

Single-mode waveguide width [μm]	1.2
Multimode waveguide width [μm]	3.3
Beat length L [μm]	39

waveguides window width of 1 μm, for the monomode arm width 1 μm and multimode waveguide width and length equal to (5.5 μm, 87 μm) and (6 μm, 102 μm), respectively. Next to it the field evolution in multimode waveguide is shown.

In Fig. 16, we present, numerically calculated by an effective index method, the dependence of propagation constant of the fundamental mode of multimode waveguide β_{M0} and the coupling length L for the self-image formation on the multimode waveguide width. Dependences obtained adapt reciprocally to the linear function. So, the phase difference defined by Eq. (12) as shown in Fig. 17 is the linear function of the waveguide width.

The same structure configuration can be used in passive shifters technology. Typically, phase shifters are made using bends increasing the waveguide lengths. We present a new type of passive MMI phase shifters based on modifying the waveguide widths. The phase delay $\Delta\phi$ of the fundamental mode for the two waveguides connected with their propagation constants difference is

$$\Delta\phi + 2n\pi = (\beta_{M0} - \beta_0)L. \tag{13}$$

The shortest length L for symmetrical excitation is $3/4 \cdot L_z$. Geometrical parameters of the π radians phase shifter optimized to work at a wavelength of 0.63 μm using silver-sodium exchanged waveguides are presented in Tab. 2. The phase shifter can be made in symmetrical configuration and asymmetrical one, for the excitation in 1/3 of the waveguide width, shown in the Fig. 18.

References

[1] SOLDANO L.B., PENNINGS E.C.M., J. Lightwave Technol. **LT-13** (1995), 615.
[2] BACHMAN M., BESSE P.A., MELCHIOR H., Appl. Opt. **33** (1994), 3905.
[3] BŁAHUT M., OPILSKI A., Opto-electronics Review **9** (2001), 293.
[4] BŁAHUT M., Opt. Appl. **29** (1999), 111.
[5] BŁAHUT M., KARASIŃSKI P., KASPRZAK D., ROGOZIŃSKI R., Opt. Commun. **214** (2002), 47.
[6] BŁAHUT M., KASPRZAK D., Opt. Appl. **33** (2003), 613.
[7] HEATON J.M., JENKINS R.M., WRIGHT D.R., PARKER J.T., BIRBECK J.C.H., HILTON K.P., Appl. Phys. Lett. **61** (1992), 1754.
[8] LAI Q., BACHMAN M., MELCHIOR H., Electron. Lett. **33** (1997), 1699.
[9] LAI Q., BACHMAN M., HUNZIKER W., BESSE P.A., MELCHIOR H., Electron. Lett. **32** (1996), 1576.
[10] SAIDA T., HIMENO A., OKUNA M., SUGITA A., OKAMOTO K., Electron. Lett. **35** (1999), 2031.
[11] DANGEL R., LUKOSZ W., Opt. Commun. **156** (1998), 63.
[12] PAIAM M.R., MACDONALD R.I., Appl. Phys. **36** (1997), 5097.
[13] LIN K.C., LEE W.Y., Electron. Lett. **32** (1996), 1259.
[14] DAS S., GERAGHTY D.F., HONKANEN S., PEYGHAMBARIAN N., Proc. SPIE **3936** (2000), 239.
[15] BŁAHUT M., Mol. Quantum Acoustics **22** (2001), 19.

Received August 18, 2004